Single particle degrees of freedom in the transition from deformed to spherical Nd nuclei

J. Holden,[1] N. Benczer-Koller,[1] G. Jakob,[1] G. Kumbartzki,[1] T. J. Mertzimekis,[1] K.-H. Speidel,[2] C. W. Beausang,[3] R. Krücken,[3] A. Macchiavelli,[4] M. McMahan,[4] L. Phair,[4] A. E. Stuchbery,[5] P. Maier-Komor,[6] W. Rogers,[7] and A. D. Davies[7]

[1]*Department of Physics and Astronomy, Rutgers University, New Brunswick, New Jersey 08903*

[2]*Institut für Strahlen- und Kernphysik, Universität Bonn, D-53115 Bonn, Germany*

[3]*A. W. Wright Nuclear Structure Laboratory, Yale University, New Haven, Connecticut 06520*

[4]*Lawrence Berkeley National Laboratory, Berkeley, California 94720*

[5]*Department of Nuclear Physics, Australian National University, Canberra ACT 0200, Australia*

[6]*Technische Universität München, D-85748 Garching, Germany*

[7]*Westmont College, Santa Barbara, California 93108*

(Received 25 September 2000; published 23 January 2001)

The g factors of the 4_1^+ and 6_1^+ states in ^{144,148}Nd, the 4_1^+ state in ^{146}Nd and the 6_1^+, 8_1^+, and 10_1^+ states in ^{150}Nd have been measured for the first time by projectile Coulomb excitation coupled to the transient field technique. The g factors of the 2_1^+ states of ^{144,146,148,150}Nd have been remeasured with high precision. The data clearly indicate that, while ^{148,150}Nd are well described by collective excitations, the structure of the low lying levels in the lighter isotopes is dominated by the $2f_{7/2}$ neutron configuration.

DOI: 10.1103/PhysRevC.63.024315 PACS number(s): 21.10.Ky, 25.70.De, 27.60.+j

I. INTRODUCTION

Recent precision measurements of magnetic moments of low lying levels of nuclei, in particular near shell closure [1–4], have highlighted the difficulties encountered by nuclear models in explaining the structure of these nuclei as a function of mass number A, spin, and energy. Large discrepancies between predictions of the standard single particle and collective models show that, for even the lowest levels, the interplay between single particle configurations and collective excitations substantially alters the structure. These effects are most noticeable in the magnetic moments. The $_{60}$Nd isotopes provide a particularly good laboratory to study these interactions, as they span a mass region which encompasses spherical, single particle nuclei near the neutron closed shell at $N=82$, vibrational and rotational nuclei.

In contrast to transition probabilities which relate to wave functions of both the initial and final states, g factors probe the microscopic structure of the individual states' wave functions. The g factors of the 2_1^+ in the Nd region have already been measured [5–9]. These measurements have demonstrated that the removal of neutrons from ^{150}Nd, lying in the middle of the $50<Z<82$ and $82<N<126$ shells, induces significant changes in the microscopic wave functions. Calculations within the framework of the IBM-II model [10,11] have been remarkably successful in describing the g factors of nuclei from Ru through Te and Ba through Os in the regions $44<Z<56$, $54<N<78$, and $56<Z<78$, $88<N<120$, albeit with some glaring discrepancies. The g factors of the Nd and Sm isotopes show a marked deviation from the prediction for the lighter isotopes. In fact, the g factors decrease with decreasing neutron number instead of increasing. As a possible resolution of the observed discrepancy in Nd and Sm, it has been proposed that the energy gap between the $1h_{11/2}$ and the $2d_{5/2}$ orbitals, large for $N<88$, yields closure of a subshell at $Z=64$. Thus, the proton bosons need to be counted from $Z=64$ and not 50 [12]. For heavier nuclei, the attractive pn interaction between the partially filled $(1h_{9/2})$ neutron orbital and the $(1h_{11/2})$ proton configuration erases the subshell gap and restores shell closure at $Z=50$. However, even this hypothesis does not resolve the discrepancies. It appears more likely that the drop in g as the closed shell $N=82$ is approached is caused by dominating single neutron configurations.

Examination of the evolution of g with spin can further highlight the impact of specific single particle configurations on the excited state's wave function. IBM-II and other collective models predict $g(4_1^+,6_1^+)\sim g(2_1^+)$.

Different scenarios need to be considered to explain the structure of the high spin and low spin ($I\leqslant 8^+$) states of these nuclei. Available g factor measurements of high spin states in $^{150}_{62}$Sm, ^{152}Gd, $^{158,164}_{66}$Dy, and $^{166,168}_{68}$Er [13–18], confirm rotational alignment of $i_{13/2}$ neutrons. Measurements of the low spin regime in $^{156}_{64}$Gd [18] and ^{166}Er [15,16] show a definite decrease of g with increasing spin. However, this effect disappears in ^{158}Gd, ^{164}Dy, and ^{168}Er [15,20] as well as in the more recent measurements on ^{156}Gd [19,20] and ^{152}Gd [17], where $g(4_1^+)\sim g(2_1^+)$. In ^{150}Sm, the isotone to ^{152}Gd, the ratio $g(4_1^+)/g(2_1^+)$ appears to be larger than unity [13,21].

Variations in the g factors of excited states have been observed near $N=8$ and $N=50$ shell closures. It is evident from measurements of the g factors of the 2_1^+ and 4_1^+ states in the O and Zr nuclei that single particle configurations play a major role in the wave functions, and as spin increases, configuration mixing decreases, and the wave functions become purer. A recent analysis of the g factors of the 2_1^+ and 4_1^+ states of ^{18,20}O and ^{92,94}Zr showed that the wave functions of these states are indeed dominated by the $d_{5/2}$ neutron configuration [4]. The ^{144,146}Nd nuclei also have two and four neutrons beyond a closed shell, namely $N=82$, where the $2f_{7/2}$ neutrons play a similar role to that of the $1d_{5/2}$ and $2d_{5/2}$ orbitals in the O and Zr nuclei, respectively. In view of these results, a measurement of the g factors of the low lying

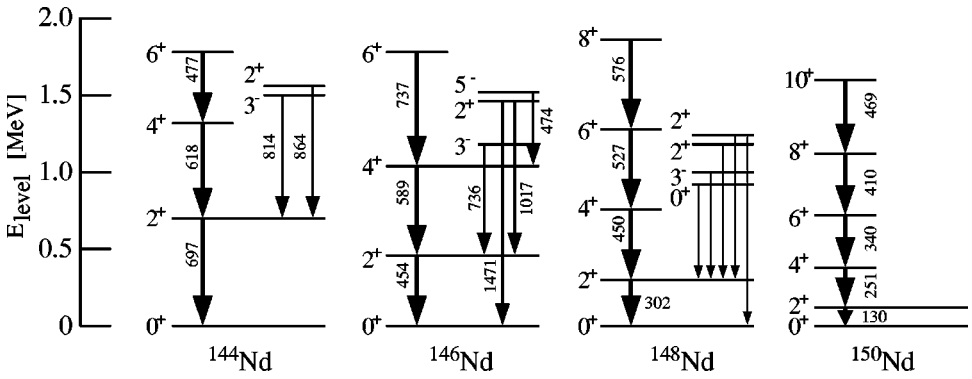

FIG. 1. Partial energy level diagram showing only levels and transitions observed in the current experiments. Unmarked transitions appearing in the spectra were identified but were not analyzed because they were too weak.

levels of the Nd isotopes becomes very interesting.

A new technique has been successfully developed, combining Coulomb excitation of heavy beams in inverse kinematics by a light target with the transient field technique [3]. This method allows for high yield and hence high precision measurements of the 2_1^+ states at low beam energies, but also large excitation of higher spin states at higher beam energies. In the present measurements, the 2_1^+ and 4_1^+ states in ^{144,146,148,150}Nd, the 6_1^+ in ^{144,148,150}Nd, and the 8_1^+ and 10_1^+ states in ^{150}Nd were populated with sufficient intensity to allow *g*-factor measurements. Partial level schemes of the isotopes studied, showing mainly the transitions observed in the present experiment, are shown in Fig. 1. The available spectroscopic information is presented in Table I [22].

II. EXPERIMENTAL TECHNIQUE

Over the past 20 years, magnetic moments of short-lived nuclear states have been measured by the transient field technique. In its conventional application, heavy target nuclei are Coulomb excited by lighter ion beams and are ejected from the target material with high velocity. If the beam ions are detected in an annular detector located at 180° with respect to the beam direction, the reaction results in alignment of the magnetic substates of the excited nuclei. These nuclei subsequently traverse a ferromagnetic material such as iron or gadolinium in which they interact with the transient magnetic field. The net effect of this interaction is a precession of the angular correlation of decay γ rays which is directly proportional to the magnetic moment of the excited state under study.

TABLE I. Spectroscopic data on the low-lying levels of ^{144,146,148,150}Nd (Ref. [22]). Energies are in units of keV, mean lives in ps, $B(E2)$'s in e^2b^2 (first line) or Weisskopf units (second line), and static quadrupole moments Q in e b (Ref. [23]).

	^{144}Nd	^{146}Nd	^{148}Nd	^{150}Nd
$E(2_1^+)$	696.5	453.8	301.7	130.2
$\tau(2_1^+)$	4.50(25)	31.2(19)	112.5(17)	2153(22)
$B(E2;2_1^+\rightarrow 0_1^+)$	0.110(6)	0.134(8)	0.276(4)	0.542(6)
	24.6(13)	29.3(17)	59.3(9)	115(1)
$Q(2_1^+)$	−0.07(15)	−0.78(9)	−1.46(13)	−2.00(51)
$E(4_1^+)$	1314.5	1042.2	752.2	381.5
$\tau(4_1^+)$	10.7(13)	5.8(14)	10.1(32)	91(4)
$B(E2;4_1^+\rightarrow 2_1^+)$	0.084(10)	0.196(48)	0.428(13)	0.820(36)
	18.8(22)	43(11)	92(3)	173(8)
$E(6_1^+)$	1791.4	1780	1279.7	720.4
$\tau(6_1^+)$		30(3) [a]		18(1)
$B(E2;6_1^+\rightarrow 4_1^+)$		0.11(1) [a]		0.991(55)
		25(3) [a]		209(12)
$E(8_1^+)$			1857	1129.7
$E(10_1^+)$				1599
$E(4_1^+)/E(2_1^+)$	1.89	2.30	2.49	2.93

[a]Reference [24].

In the present experiment, it is the heavy beam ion that is Coulomb excited by a lighter target nucleus. The excited projectiles traverse the ferromagnetic layer where they experience the spin precession in the transient magnetic hyperfine field before they stop in a backing of the target made of a cubic medium, where no further interaction takes place. The light target ions are scattered forward and need to have sufficient energy to exit the target and the beamstop. They are detected in a detector located at 0° with respect to the beam. The measurement of the γ rays emitted by excited projectiles in coincidence with the target nuclei is an essential element of the technique. It ensures that the observed γ rays originate from excitations in the target and from states with good alignment. The requirements for the light target material are threefold: sufficient excitation of the projectiles, sufficient energy after the collision to traverse all the target layers as well as the beamstop, and low target excitation with deexcitation γ rays of energies different from those of the projectile γ rays. Due to the kinematic focusing, the technique ensures high efficiency for detection of the reaction products in the forward direction, allowing access to weakly populated higher spin states, as well as providing the high velocity of the recoiling ions essential for transient field measurements. The technique has the advantage of keeping the experimental conditions fairly constant for different isotopes, including the use of the *same* target for each isotope, and thus allows for very accurate *relative* measurements.

The technique of Coulomb excitation of beams provided by the ion source of the accelerator combined with transient fields has been successfully applied to the measurement of *g* factors of the light and medium heavy nuclei ^{46,48}Ti, ^{50,52}Cr [1,2], ^{74,76,78,80,82}Se [3], and ^{92,94}Zr [4]. The present work represents the first application of the technique to heavy systems in the $A=150$ region.

TABLE II. Description of the composition of the multilayered targets. All thicknesses are given in mg/cm^2. WNSL and LBNL refer to the targets used at Yale and Berkeley, respectively. M is the magnetization of the target in Tesla. An additional copper foil of 7.5 or 8.9 mg/cm^2 was placed behind the target to stop the beam in the WNSL and LBNL experiments, respectively.

	Ni	Si	Gd	Ta	Al	Cu	M
WNSL	-	0.95	4.4	1.0	1.35		0.1670
LBNL	1.0	-	5.5	1.0	-	5.3	0.1870

The experimental details for measuring magnetic moments of short-lived excited states by the transient field technique in both standard [25] and inverse kinematics [3] have been described in previous publications. Only details pertaining to the current measurements are presented here. Two sets of experiments were carried out. Isotopic beams of ^{144,146,148,150}Nd near 285 MeV were provided by the Wright Nuclear Structure Laboratory (WNSL) ESTU tandem Van de Graaff accelerator at Yale University. Only the 2_1^+ states were excited at these beam energies. The resulting $g(2_1^+)$ factors provided a consistency check for the use of inverse kinematics as well as for the determination of the transient field strength. The higher spin states were measured at the Lawrence Berkeley National Laboratory (LBNL), where isotopic beams of ^{144,146,148,150}Nd were accelerated to between 584 and 608 MeV by the 88 Inch Cyclotron.

Energies and target specifications were chosen to keep the velocities of the beam ions within the gadolinium foil comparable to those at lower beam energies, and to allow the cyclotron to switch beams with relative ease. Since these energies are close to the Coulomb barrier for Nd on Ni targets, $E_B \sim 650$ MeV, particle transfer reactions can also take place. For instance, the $(3/2)^- \rightarrow (1/2)^-$ transition from ^{143}Nd, produced in neutron transfer from ^{144}Nd was observed at the beam energy at which the experiment was run. The major findings of the Berkeley experiments were reported in a short publication [26].

Two different targets were used for the low and high energy experiments. Each of these targets consisted of several layers. Natural Si or Ni layers were deposited on a gadolinium substrate, itself evaporated on a tantalum foil heated to 800 K. A copper or aluminum backing stopped the excited beam ions. An additional copper foil was placed behind each of the targets to stop the beam. The details of the target layers are summarized in Table II.

TABLE III. Characteristics of the reaction kinematics. $\langle E \rangle_{\rm in}$, $\langle E \rangle_{\rm out}$, $\langle v/v_0 \rangle_{\rm in}$, and $\langle v/v_0 \rangle_{\rm out}$ are, respectively, the average energies and velocities of the ^{A}Nd isotopes as they enter into and exit from the gadolinium layer. Energies are given in MeV; $v_0 = e^2/\hbar$ is the Bohr velocity.

		$E_{\rm beam}$	$\langle E \rangle_{\rm in}$	$\langle E \rangle_{\rm out}$	$\langle v/v_0 \rangle_{\rm in}$	$\langle v/v_0 \rangle_{\rm out}$
WNSL	^{144}Nd	288	92.6	23.2	5.09	2.55
	^{146}Nd	286	93.1	23.8	5.07	2.56
	^{148}Nd	284	93.6	24.3	5.05	2.57
	^{150}Nd	282	94.0	24.8	5.03	2.58
LBNL	^{144}Nd	608	86.2	12.7	4.91	1.89
	^{146}Nd	600	87.5	13.4	4.91	1.92
	^{148}Nd	592	88.9	14.1	4.92	1.96
	^{150}Nd	584	89.6	14.5	4.91	1.97

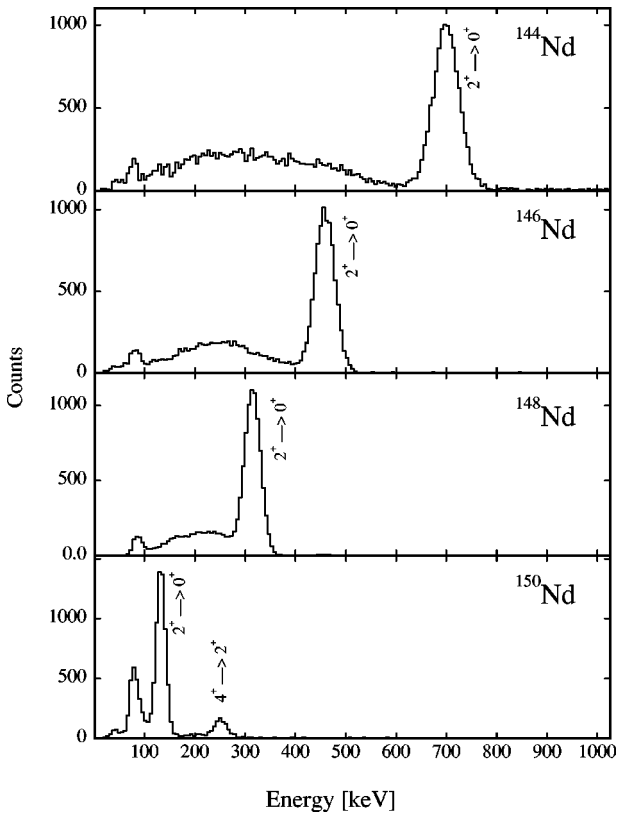

FIG. 2. NaI(Tl) spectra of ^{144,146,148,150}Nd γ rays in coincidence with forward scattered Si target ions observed in the WNSL experiments.

The thicknesses of the target layers were chosen to ensure that the excited Nd ions traversed the gadolinium layer with a velocity $2v_0 \leqslant v \leqslant 6v_0$, where $v_0 = e^2/\hbar$ is the Bohr velocity. The specifics of the reaction kinematics are presented in Table III.

The WNSL target was cooled to ~50 K by a closed-cycle helium refrigerator, while at LBNL, the target and beam stop were mounted on the tip of a liquid nitrogen dewar and maintained at a temperature of ~77 K. In both cases, the temperature was monitored with a thermocouple connected to the target frame.

The magnetizations of the targets were measured in an AC magnetometer [27] before and after each experiment. The magnetization was effectively constant between 40 K and 100 K and did not change as a result of the bombardment. During the experiment an external magnetic field of 0.06 T was applied to the target to magnetize the gadolinium foil. The field direction, perpendicular to the γ-ray detection plane, was changed every 3–5 min. The recoiling target ions were detected by a 100 μm thick passivated implanted planar silicon detector placed at 0°, 28 mm away from the target. The particle detector subtended an angle of $\pm 19°$, corre-

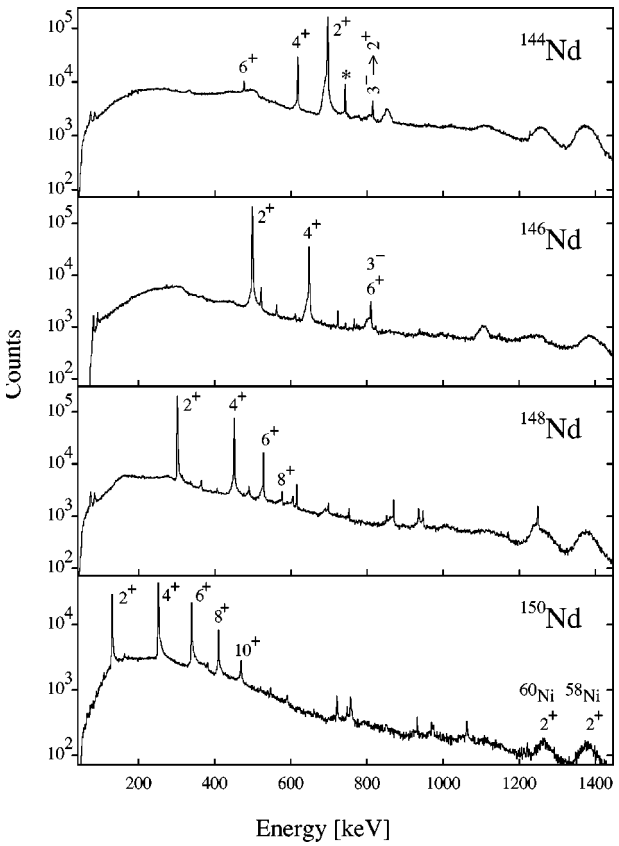

FIG. 3. Ge spectra of ^{144,146,148,150}Nd γ rays in coincidence with forward scattered Ni target ions observed in the LBNL experiments. The γ transitions are labeled by the spins of the state of origin. The line marked by an asterisk corresponds to a transition in ^{143}Nd. The degeracy of the 6^+ and 3^- lines in ^{146}Nd is discussed in the text.

sponding, for example, in the case of ^{144}Nd, to a ^{144}Nd recoil angular range of $\pm 20°$. The γ rays were detected in coincidence with the Si or Ni ions.

In the experiments at WNSL, four 12.7 cm$\times$12.7 cm NaI(T*l*) scintillators at distances of 17 cm from the target position were used. The detectors were positioned at $\pm 66°$ and $\pm 114°$ with respect to the beam direction for the precession measurements. A Ge detector was included in the setup to ensure the absence of any interfering γ lines in the spectra. In the LBNL experiments, Ge detectors had to be used to resolve the transitions from higher spin states. Hence, four Ge detectors of approximately 25% efficiency, located 6.8 cm away from the target, were positioned at $\pm 62°$ and $\pm 118°$ with respect to the beam direction during the precession measurements. Typical spectra are shown in Figs. 2 and 3.

The γ-ray anisotropies have been measured in both the WNSL and LBNL experiments. For these, pairs of detectors were placed, alternately, at angles close to $\pm 45°$ or $\pm 135°$ and $\pm 90°$.

III. DATA ANALYSIS

The measured precession effect ϵ for the radiation deexciting a certain state can be expressed as [3]

TABLE IV. Average experimental ratios $\langle R \rangle$ and slopes $S(62°)$ of the $2_1^+ \rightarrow 0_1^+$ transitions showing the attenuation resulting from paramagnetic effects (Ref. [7] and WNSL measurements). The lifetimes are from Ref. [22].

	τ(ps)	$\langle R \rangle$	$S(62°)$
^{144}Nd	6.5(4)	7.66(36)	−2.26(2)
^{146}Nd	31.2(19)	6.36(17)	−2.17(1)
^{148}Nd	112.5(17)	4.54(7)	−1.96(1)
^{150}Nd	2153(22)	1.45(3)	−0.63(3)

$$\epsilon = \frac{\rho - 1}{\rho + 1}, \tag{3.1}$$

where $\rho = (\rho_{14}/\rho_{23})^{1/2}$ is determined from the double ratios

$$\rho_{ij} = \left(\frac{N_i^{\uparrow}/N_i^{\downarrow}}{N_j^{\uparrow}/N_j^{\downarrow}} \right)^{1/2}, \tag{3.2}$$

where the coefficients $i,j = 1,2,3,4$ represent the four detectors; $N_{i,j}^{\uparrow}$ and $N_{i,j}^{\downarrow}$ are the coincidence counting rates of the photopeak of the γ transition in the ith or jth detector with the external field pointing ''up'' ($\uparrow$) or ''down'' ($\downarrow$) with respect to the γ-ray detection plane. The γ-ray photopeak intensities have been corrected for random and background rates. Calculations were carried out in the center of mass system. Similar ''cross ratios'' $\rho_c = (\rho_{24}/\rho_{13})^{1/2}$ and ϵ_c were calculated to check for systematic effects that might mask the true precession. In all cases, vanishingly small ϵ_c values were obtained, as expected. The precession angles $\Delta\theta$ are derived from the measured ϵ's through the relationship

$$\Delta\theta = \epsilon / S, \tag{3.3}$$

where $S(\theta_0) = [1/W(\theta_0)] \cdot [dW(\theta)/d\theta]|_{\theta=\theta_0}$ is the logarithmic slope of the angular correlation at the angles of interest θ_0.

The unperturbed angular correlations measured previously [7,8] showed an attenuation of the correlations of the $2_1^+ \rightarrow 0_1^+$ transitions in ^{148,150}Nd which has been attributed to paramagnetic effects resulting from the long lifetimes of the 2_1^+ states in these isotopes. In the Yale experiments, the slopes of the $2_1^+ \rightarrow 0_1^+$ transitions in ^{144,146,148,150}Nd were derived as described in [28] from the measured ratios of counts in pairs of detectors,

TABLE V. Logarithmic slopes $S(62°)$ calculated from the COULEX code for the LBNL experimental conditions.

	$2_1^+ \rightarrow 0_1^+$	$4_1^+ \rightarrow 2_1^+$	$6_1^+ \rightarrow 4_1^+$	$8_1^+ \rightarrow 6_1^+$	$10_1^+ \rightarrow 8_1^+$
^{144}Nd	-1.96	-0.885	-0.720		
^{146}Nd	-1.90	-0.841	-0.691		
^{148}Nd	-2.02 [a]	-0.904	-0.729		
^{150}Nd		-0.859	-0.701	-0.645	-0.617

[a]This value includes the correction for the attenuation due to paramagnetic effects.

TABLE VI. Relative level populations, in percent. Missing values imply that the level has negligible excitation. The 2^+ state at $E_{exc}=1.3032$ MeV in ^{146}Nd was not observed (Ref. [22]); the 2^+ at $E_{exc}=1.4706$ MeV was excited and appears in the table as 2_2^+.

	2_1^+	4_1^+	3_1^-	2_2^+	5_1^-	6_1^+	8_1^+	10_1^+
^{144}Nd	77.0	12.3	2.8	6.6	-	1.4	-	-
^{146}Nd	60.6	28.1	3.9	4.9	1.6	0.8	-	-
^{148}Nd	36.3	46.6	-	-	-	17.0	-	-
^{150}Nd	0	33.8	-	-	-	39.0	18.5	8.7

$$R(45°/88°)=\left(\frac{N_i(45°)N_j(45°)}{N_i(88°)N_j(88°)}\right)^{1/2} \quad \text{and}$$

$$R(135°/92°)=\left(\frac{N_i(135°)N_j(135°)}{N_i(92°)N_j(92°)}\right)^{1/2}.$$

The average of these ratios, $\langle R\rangle$, and the resulting slopes are displayed in Table IV. The measured dependence of the attenuation of the slope of the angular correlation with lifetime of the state is in agreement with the observations of previous measurements [7].

Similar data were obtained for the LBNL measurements. However, the extraction of slopes was complicated by absorption effects in the experimental layout at the angles where the anisotropies were measured. The ensuing necessary corrections increased the experimental uncertainties. Therefore, the angular correlations $W(\theta)$ were calculated from the Winther-deBoer COULEX code, and the derived slopes are shown in Table V. The $W(\theta)$'s reflect the excited state's spin alignment, which, in turn, depends primarily on the acceptance angle of the coincidence particle detector, and only weakly on the transition matrix elements. These, unfortunately, are not known for many of the higher spin states. In these cases, the $B(E2;I\rightarrow I-2)$ for the unknown state was assumed to be equal to that of the state below it. It is noteworthy that varying the $B(E2)$'s by as much as a factor of four had a negligible effect on the calculated slopes. In addition, the theoretical slope of the $2_1^+\rightarrow 0_1^+$ transition in ^{148}Nd was corrected for the attenuation due to paramagnetism as determined from the low energy data obtained at Yale. Since in all cases, the experimental slopes were in agreement with the theoretical calculations within experimental errors, the theoretical slopes were adopted for the analysis of the precession data.

The determination of the precession angles $\Delta\theta$ of the highest excited state in each isotope follows directly from the measured precession and the slope of the angular correlation. However, the determination of the precession angle $\Delta\theta$ for the lower states, in particular the 2_1^+ states, required a more elaborate analysis due to significant contributions to the observed precession due to feeding from the precursor states (Fig. 1). The precessions of the higher states, which must be taken into account explicitly, are characterized by the population strength and the appropriate angular correlations.

Since the population of the 2_1^+ states due to feeding is dominated by stretched $E2$ transitions within the ground state bands, the measured effects ϵ for the 2_1^+ states can be expressed as [3]

$$\epsilon_{2_1^+}^{\text{meas}}=\frac{\sum_i \epsilon_i P_i W_i(\theta_0)}{\sum_i P_i W_i(\theta_0)}, \tag{3.4}$$

where ϵ_i is the precession effect that would be observed for a directly excited ith state, $W_i(\theta_o)$ is the angular correlation function at the angle θ_0 of the ith transition, and P_i represents the population strength of the ith state which is proportional to the total Coulomb excitation cross section for that state. At high beam energies, a substantial portion of the strength of the lower state's population is fed in the decay from higher states, thus limiting the precision with which $g(2_1^+)$ can be measured. This limitation is especially significant for the heavier Nd isotopes, which have high excitation probabilities for the higher spin states, precluding a measurement of $g(2_1^+)$ in ^{150}Nd.

The populations P_i of each of the states can be determined from COULEX calculations of the cross sections. Such calculations depend on the input of reliable transition matrix elements. As $B(E2)$'s are not known for many of the states of interest in this work, level populations had to be measured. The relative intensity of all transition lines was determined from the γ spectra of the precession runs at $\pm 62°$, $\pm 118°$. This intensity was corrected for relative efficiency of the Ge detector, absorption, internal electron conversion, and the calculated theoretical angular correlation, including the feeding from higher states. The populations of each of the states were then obtained (with negligible statistical uncertainties), and are shown in Table VI.

The precession angles $\Delta\theta$ can now be derived from the measured ϵ values and the determined $S_i(\theta_0), P_i$, and $W_i(\theta_0)$. The results are summarized in Table VII.

TABLE VII. Measured precession angles $-\Delta\theta$(rad).

	$\Delta\theta(2_1^+\rightarrow 0_1^+)$	$\Delta\theta(4_1^+\rightarrow 2_1^+)$	$\Delta\theta(6_1^+\rightarrow 4_1^+)$	$\Delta\theta(8_1^+\rightarrow 6_1^+)$	$\Delta\theta(10_1^+\rightarrow 8_1^+)$
^{144}Nd	0.0239(8)	0.0159(43)	–0.069(28)	-	
^{146}Nd	0.0358(10)	0.0226(30)(8) [a]	-	-	
^{148}Nd	0.0392(16)	0.0424(29)	0.0292(56)	-	
^{150}Nd	-	0.056(9)	0.043(8)	0.061(17)	0.016(21)

[a]The second error in $\Delta\theta(4_1^+)$ arises from the assumption $-0.3\leqslant g(^{146}\text{Nd};6_1^+)\leqslant 0.3$ (see text).

TABLE VIII. Comparison of the previous and current $g(2_1^+)$ factors of the Nd isotopes.

Year	^{144}Nd	^{146}Nd	^{148}Nd	^{150}Nd
1978 [6] [a]	+0.19(2)	+0.30(2)	+0.34(2)	-
1987 [7]	+0.166(41)	+0.312(49)	+0.411(42)	+0.418(38)
1990 [8]	+0.16(2)	+0.29(1)	+0.35(2)	+0.41(3)
WNSL	+0.189(22)	+0.302(21)	+0.356(14)	+0.48(12)
LBNL	+0.209(7)	+0.289(8)	+0.363(14)	-

[a]Results reevaluated for new field calibration as discussed in [8].

A complication in ^{146}Nd arises from the fact that the energy of the $(6_1^+ \rightarrow 4_1^+)$ transition is identical to that of the $(3_1^- \rightarrow 2_1^+)$ transition (Fig. 1). Not only is the ability to determine $g(^{146}\text{Nd};\ 6_1^+)$ affected, but also $g(4_1^+)$ and $g(2_1^+)$, since the feeding contributions from the 6_1^+ and 3_1^- states are different. An auxiliary experiment was carried out using the 8π detector array at LBNL to determine the relative populations of the 6_1^+ and 3_1^- states [29]. A 600 MeV beam of ^{146}Nd was directed at a thick $^{\text{nat}}$Ni target, and γ-γ coincidence data were recorded. From the ratio of the intensities of the $(4_1^+ \rightarrow 2_1^+)$ and $(2_1^+ \rightarrow 0_1^+)$ γ-ray lines in coincidence with the $(6_1^+ \rightarrow 4_1^+)+(3_1^- \rightarrow 2_1^+)$ transitions, it was found that $(17 \pm 0.5)\%$ of the intensity belonged to the 6_1^+ state. Without knowing the g factor of at least one of these states, it is impossible to determine the g factor of the other. However, limits based on extrapolation from the results of the ^{144,148}Nd data can be placed on the g factors of the lower spin states with the assumption that $-0.3 \leqslant g(6_1^+) \leqslant 0.3$. The 2_1^+ state is so strongly populated directly that the uncertainty in $g(6_1^+)$ within this range has a negligible effect. Since the contribution from the 6_1^+ state is so small, and the 4_1^+ state is not fed by the 3_1^- state, the range of possible $g(4_1^+)$ given the assumption for the range of $g(6_1^+)$ values is comparable to the size of the statistical error.

IV. RESULTS

The g factors are finally determined from the expression

$$\Delta\theta = -g\frac{\mu_N}{\hbar}\int_{t_{\text{in}}}^{t_{\text{out}}} B(v(t),Z)e^{-t/\tau}dt, \qquad (4.1)$$

where B, the transient field, is a function of the velocity v and atomic number Z of the projectile ion, τ is the mean lifetime of the state being examined, and t_{in} and t_{out} are the mean entrance and exit times of the ions into or out of the ferromagnet. The Rutgers parametrization of the transient field was used [30]. The resulting $g(2_1^+)$ factors are compared with previous measurements in Table VIII. The quoted errors are statistical in all cases. The WNSL g factor results are in excellent agreement with those of previous measurements [6–8], a result particularly gratifying given that the current measurements use a different technique and gadolinium as the ferromagnet instead of iron. The LBNL $g(2_1^+)$ data obtained at higher beam energies are also in good agreement with the previous data.

TABLE IX. g factors of low-lying states in the Nd isotopes. The $g(2_1^+)$ values are the averages of all the data listed in Table VIII. The g factors of the higher spin states are the results of the LBNL experiment only, with the exception of $g(4_1^+)$ of ^{150}Nd, which is the average of the present result, $g(4_1^+) = +0.45(7)$ and the value of Ref. [8], $g(4_1^+) = +0.44(4)$. The quoted errors are statistical. The second error listed for $g(4_1^+)$ in ^{146}Nd has its origin in the unresolvable degeneracy of the $6_1^+ \rightarrow 4_1^+$ and $3_1^- \rightarrow 2_1^+$ transitions as discussed in the text.

	^{144}Nd	^{146}Nd	^{148}Nd	^{150}Nd
2_1^+	+0.201(6)	+0.291(6)	+0.357(8)	+0.42(2)
4_1^+	+0.131(36)	+0.193(26)(6)	+0.360(25)	+0.44(3)
6_1^+	−0.56(22)	-	+0.266(51)	+0.35(7)
8_1^+	-	-	-	+0.56(13)
10_1^+	-	-	-	+0.14(19)

The $g(I)$ factors obtained are shown in Table IX and Fig. 4. It should be noted that while the absolute g factors are subject to certain systematic uncertainties, such as may result from the parametrization of the transient field, the *relative g* factors are not. The current measurements were obtained with a single target under nearly identical experimental conditions. Beam energies, for example, were adjusted so that the Nd ions of each isotope entered and exited the Gd foil with the same velocities. Thus, any systematic effects would alter the results equally, maintaining the trends in the g factors as a function of neutron number and angular momentum.

V. DISCUSSION

^{150}Nd is a classical rotational nucleus, with prolate deformation, as evidenced by the unambiguous signature of the ratio $E(4_1^+)/E(2_1^+) = 2.93$, the static quadrupole moment of the 2_1^+ state, $Q = -2.00(51)$ e b, and the $B(E2;2_1^+ \rightarrow 0_1^+) = 115$ W.u. For such a nucleus, it is expected that the g factors of all the states in the rotational band will be equal and near $Z/A = 0.4$, a prediction confirmed by the data.

The data show that as neutrons are removed and N approaches the magic number 82, the g factors decrease continuously, as do the $B(E2;2_1^+ \rightarrow 0_1^+)$'s (Table I) and the

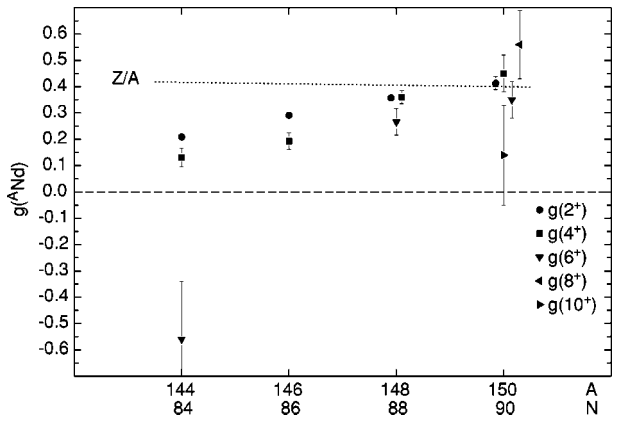

FIG. 4. Summary of the measured $g(I)$ factors as a function of mass number A or neutron number N.

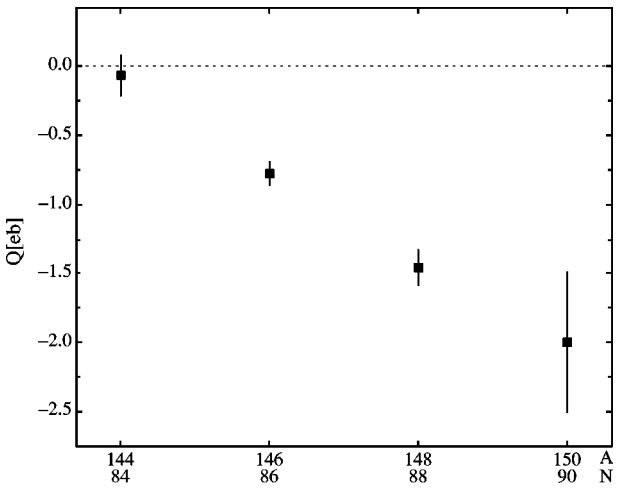

FIG. 5. Summary of the measured static quadrupole moments Q (Ref. [23]).

magnitudes of the static quadrupole moments Q (Fig. 5).

The present spin dependence of the g factors, in particular for ^{144}Nd for which $g(6_1^+)$ is negative, shows clearly that the low-excitation structure of this nucleus is dominated by the $2f_{7/2}$ neutron configuration. The progression of g with neutron number occupation reflects a decreasing contribution of the $2f_{7/2}$ neutron configuration as the nuclei become more collective. The same effect is seen in the odd isotopes ^{143}Nd and ^{145}Nd for which the g factors of the $(7/2)^-$ ground states have been measured, $g(^{143}\mathrm{Nd}) = -0.304(1)$ and $g(^{145}\mathrm{Nd}) = -0.187(1)$, respectively [31]. The Schmidt limit value for a $f_{7/2}$ neutron is -0.547 using $g_s = g_s^{\mathrm{free}} = -3.826$.

Lombard [32] carried out a calculation which included a single-particle microscopic description of the 2_1^+ states of spherical even-even nuclei with the residual interaction between nucleons being represented by a pairing-plus-quadrupole force. The contributions to the magnetic moments arise primarily from the configuration mixing of single particle states near the Fermi surface. The calculations yield $g(^{144}\mathrm{Nd}) = +0.11$, $g(^{146}\mathrm{Nd}) = +0.13$, and $g(^{148}\mathrm{Nd}) = +0.16$, a correct trend for the lighter isotopes, but not reflective of the sharp rise for the nuclei closer to the deformed region, not surprising since the theory ignores deformation of the core.

Calculations [33] in the framework of the cranked Hartree-Fock-Bogoliubov formalism with the inclusion of hexadecapole deformation do not reproduce the measured g factors. Similarly, IBA-II models fail to reproduce the data, especially the spin dependence of the g factors of ^{144,146}Nd.

A relatively simple model based on the microscopic calculation of pair gaps and evaluation of g factors in the Migdal approximation [34] accurately predicts the mass dependent variation of the collective g factors in ^{146,148,150}Nd. This approach, however, does not account for the reduced g factors of higher spin states in ^{144}Nd and ^{146}Nd, or for the further drop in $g(2_1^+)$ in the progression from ^{146}Nd to ^{144}Nd. Recent shell model calculations [35] have been carried out with the protons limited to the $1g_{7/2}$ and $2d_{5/2}$ orbits (which effectively assumes closure at $Z=64$) and the additional neutron in the $2f_{7/2}$ and $2p_{3/2}$ orbits. This calculation gives a reasonably good account of the level spectra but predicts that the g factors of the 2_1^+, 4_1^+, and 6_1^+ states in ^{144}Nd are all negative, near the value of a neutron $f_{7/2}$ configuration.

Calculations involving the coupling of valence nucleons to a collective core [24,36] have been carried out for ^{144}Nd. These calculations, which predict reasonably well the energies and $B(E2)$'s, require a considerable $(2f_{7/2})^2$ neutron strength which increases with spin, as required by the observed g factors. Although the theoretical g factor of the 2_1^+ state in ^{144}Nd [36] is somewhat smaller than the experimental result, these calculations give, in general, a much better description of the data than does the shell model with a limited configuration space. A large configuration space shell model calculation is needed to understand quantitatively the change in structure in the transition from ^{150}Nd to ^{144}Nd. However, as was noted in recent work on the g factors in the Mo isotopes near $N=50$ [37], it may not be sufficient to simply extend the basis space to account quantitatively for the low-spin g factors which are also sensitive to the choice of two-body matrix elements, especially the proton-neutron interactions. The present g factor data are therefore important to determine the effective residual interactions in this region which, at present, are not well known.

ACKNOWLEDGMENTS

The authors acknowledge the support of the U.S. National Science Foundation, the Department of Energy Grant No. DE-FG02-91ER-40609, the BMBF, and the Deutsche Forschungsgemeinschaft. The work was also supported by the Director, Office of Energy Research, Division of Nuclear Physics of the Office of High Energy and Nuclear Physics of the Department of Energy under Contract No. DE-AC03-76SF00098. K.-H.S. thanks the Rutgers University Nuclear Physics Laboratory for hosting summer visits during 1998–2000. W.F.R. and A.D.D. acknowledge the support of the U.S. National Science Foundation Grant No. PHY97-22602. A.E.S. acknowledges the support of the Australian Academy of Science International Exchange Program.

[1] R. Ernst, K.-H. Speidel, O. Kenn, U. Nahum, J. Gerber, P. Maier-Komor, N. Benczer-Koller, G. Jakob, G. Kumbartzki, L. Zamick, and F. Nowacki, Phys. Rev. Lett. **84**, 416 (2000).

[2] K.-H. Speidel, R. Ernst, O. Kenn, J. Gerber, P. Maier-Komor, N. Benczer-Koller, G. Kumbartzki, L. Zamick, M. S. Fayache, and Y. Y. Sharon, Phys. Rev. C **62**, 031301(R) (2000).

[3] K.-H. Speidel, N. Benczer-Koller, G. Kumbartzki, C. Barton, A. Gelberg, J. Holden, G. Jakob, N. Matt, R. H. Mayer, M. Satteson, R. Tanczyn, and L. Weissman, Phys. Rev. C **57**, 2181 (1998).

[4] G. Jakob, N. Benczer-Koller, J. Holden, G. Kumbartzki, T. J. Mertzimekis, K.-H. Speidel, C. W. Beausang, and R. Krüken, Phys. Lett. B **468**, 13 (1999).
[5] H. W. Kugel, R. R. Borchers, and R. Kalish, Nucl. Phys. **A186**, 513 (1972).
[6] R. Kalish, A. G. De Raedt, A. Holthuizen, W. A. Sterrenburg, and G. van Middelkoop, Nucl. Phys. **A311**, 507 (1978).
[7] N. Benczer-Koller, D. J. Ballon, and A. Pakou, Hyperfine Interact. **33**, 37 (1987).
[8] A. E. Stuchbery, G. J. Lampard, and H. H. Bolotin, Nucl. Phys. **A516**, 119 (1990).
[9] D. Bazzacco, F. Brandolini, K. Löwenich, P. Pavan, C. Rossi-Alvarez, and E. Maglione, Nucl. Phys. **A533**, 541 (1991).
[10] M. Sambataro, O. Scholten, A. E. L. Dieperink, and G. Piccitto, Nucl. Phys. **A423**, 333 (1984).
[11] M. Sambataro and A. E. L. Dieperink, Phys. Lett. **107B**, 249 (1981).
[12] A. Wolf, D. D. Warner, and N. Benczer-Koller, Phys. Lett. **158B**, 7 (1985).
[13] T. Vass, A. W. Mountford, G. Kumbartzki, N. Benczer-Koller, and R. Tanczyn, Phys. Rev. C **48**, 2640 (1993).
[14] G. Seiler-Clark, D. Pelte, H. Emling, A. Balanda, H. Grein, E. Grosse, R. Kulessa, D. Schwalm, H. J. Wollersheim, M. Hass, G. J. Kumbartzki, and K.-H. Speidel, Nucl. Phys. **A399**, 211 (1983).
[15] C. E. Doran, A. E. Stuchbery, H. H. Bolotin, A. P. Byrne, and G. J. Lampard, Phys. Rev. C **40**, 2035 (1989); C. E. Doran, H. H. Bolotin, A. E. Stuchbery, and A. P. Byrne, Z. Phys. A **325**, 285 (1986).
[16] A. Alzner, E. Bodenstedt, B. Gemünden, J. van den Hoff, and H. Reif, Z. Phys. A **322**, 467 (1985).
[17] N. A. Matt, N. Benczer-Koller, J. Holden, G. Kumbartzki, R. H. Mayer, M. Satteson, and R. Tanczyn, Phys. Rev. C **59**, 665 (1999).
[18] A. Alzner, E. Bodenstedt, B. Gemünden, J. van den Hoff, S. Piel, R. Sajok, H. Koch, Th. Schäfer, and R. Vianden, Z. Phys. A **331**, 277 (1988); Th. Schäfer, R. Vianden, and E. Boden stedt, *ibid.* **335**, 387 (1990).
[19] A. E. Stuchbery, A. G. White, G. D. Dracoulis, K. J. Schiffer, and B. Fabricius, Z. Phys. A **338**, 135 (1991).
[20] F. Brandolini, P. Pavan, D. Bazzacco, C. Rossi-Alvarez, R. V. Ribas, M. de Poli, and A. M. I. Haque, Phys. Rev. C **45**, 1549 (1992).
[21] A. P. Byrne, A. E. Stuchbery, H. H. Bolotin, C. E. Doran, and G. J. Lampard, Nucl. Phys. **A446**, 419 (1987).
[22] J. K. Tuli, Nucl. Data Sheets **56**, 607 (1989); L. K. Peker, *ibid.* **82**, 187 (1997); **59**, 393 (1990); E. derMateosian and J. K. Tuli, *ibid.* **75**, 827 (1995). Data extracted from the ENSDF database, version (9-Aug-2000), [NNDC].
[23] H. S. Gertzman, D. Cline, H. E. Gove, and P. M. S. Lesser, Nucl. Phys. **A151**, 282 (1971).
[24] S. J. Robinson, B. Faircloth, P. Miočinović, and A. S. Altgilbers, Phys. Rev. C **62**, 044306 (2000).
[25] N. Benczer-Koller, M. Hass, and J. Sak, Annu. Rev. Nucl. Part. Sci. **30**, 53 (1980).
[26] J. Holden, N. Benczer-Koller, G. Jakob, G. Kumbartzki, T. J. Mertzimekis, K.-H. Speidel, A. Macchiavelli, M. McMahan, L. Phair, P. Maier-Komor, A. E. Stuchbery, W. F. Rogers, and A. D. Davies, Phys. Lett. B **493**, 7 (2000).
[27] A. Piqué, J. M. Brennan, R. Darling, R. Tanczyn, D. Ballon, and N. Benczer-Koller, Nucl. Instrum. Methods Phys. Res. A **279**, 579 (1989).
[28] R. Ernst, K.-H. Speidel, O. Kenn, A. Gohla, U. Nahum, J. Gerber, P. Maier-Komor, N. Benczer-Koller, G. Kumbartzki, L. Zamick, and F. Nowacki, Phys. Rev. C **62**, 024305 (2000).
[29] W. Rogers, A. D. Davies, J. Holden, A. Macchiavelli, P. Fallon, and D. Ward (private communication).
[30] N. K. B. Shu, D. Melnik, J. M. Brennan, W. Semmler, and N. Benczer-Koller, Phys. Rev. C **21**, 1828 (1980).
[31] P. Raghavan, At. Data Nucl. Data Tables **42**, 189 (1989).
[32] R. J. Lombard, Nucl. Phys. **A114**, 449 (1968).
[33] Ramendra Nath Majumdar, Phys. Rev. C **61**, 064312 (2000).
[34] A. E. Stuchbery, Nucl. Phys. **A589**, 222 (1995).
[35] A. E. Stuchbery, Nuclear Structure 2000 Conference, 2000, East Lansing, Michigan; A. E. Stuchbery and N. Benczer-Koller (to be published).
[36] J. Copnell, S. J. Robinson, J. Jolie, and K. Heyde, Phys. Rev. C **46**, 1301 (1992).
[37] P. F. Mantica, A. E. Stuchbery, D. E. Groh, J. I. Prisciandaro, and M. P. Robinson (to be published).